Benchmark study on methanol C–H and O–H bond activation by bare [Fe IVO]2+

ARTICLE *in* THE JOURNAL OF PHYSICAL CHEMISTRY A · AUGUST 2014

Impact Factor: 2.69 · DOI: 10.1021/jp505662x · Source: PubMed

5 AUTHORS, INCLUDING:

Xiaoli Sun
Jilin University
9 PUBLICATIONS **46** CITATIONS
SEE PROFILE

Jilai Li
Jilin University
66 PUBLICATIONS **287** CITATIONS
SEE PROFILE

THE JOURNAL OF PHYSICAL CHEMISTRY A

Article

pubs.acs.org/JPCA

Benchmark Study on Methanol C−H and O−H Bond Activation by Bare $[Fe^{IV}O]^{2+}$

Xianhui Sun,[†,∥] Xiaoli Sun,[†,∥] Caiyun Geng,[†] Haitao Zhao,[‡] and Jilai Li*[,†,§]

[†]State Key Laboratory of Theoretical and Computational Chemistry, Institute of Theoretical Chemistry, Jilin University, Changchun 130023, P.R. China

[‡]Department of Chemistry, School of Science, Tianjin University, Tianjin, 300072, China

Supporting Information

ABSTRACT: We present a high-level computational study on methanol C−H and O−H bond cleavages by bare $[Fe^{IV}O]^{2+}$, as well as benchmarks of various density functional theory (DFT) methods. We considered direct and concerted hydrogen transfer (DHT and CHT) pathways, respectively. The potential energy surfaces were constructed at the CCSD(T)/def2-TZVPP//B3LYP/def2-TZVP level of theory. Mechanistically, (1) the C−H bond cleavage is dominant and the O−H activation only plays minor role on the PESs; (2) the DHT from methyl should be the most practical channel; and (3) electronic structure analysis demonstrates the proton and electron transfer coupling behavior along the reaction coordinates. The solvent effect is evident and plays distinct roles in regulating the two bond activations in different mechanisms during the catalysis. The effect of optimizing the geometries using different density functionals was also studied, showing that it is not meaningful to discuss which DFT method could give the accurate prediction of the geometries, especially for transition structures. Furthermore, the gold-standard CCSD(T) method was used to benchmark 19 different density functionals with different Hartree−Fock exchange fractions. The results revealed that (i) the structural factor plays a minor role in the single point energy (SPE) calculations; (ii) reaction energy prediction is quite challenging for DFT methods; (iii) the mean absolute deviations (MADs) reflect the problematic description of the DFs when dealing with metal oxidation state change, giving a strong correlation on the HF exchange in the DFs. Knowledge from this study should be of great value for computational chemistry, especially for the *de novo* design of transition metal catalysts.

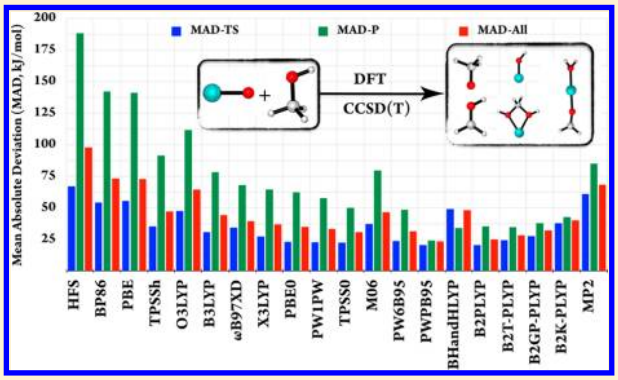

1. INTRODUCTION

The methanol synthesis process is highly important due to its potential applications in various fields. For example, methanol is widely used as the cheapest resource in direct methanol fuel cells (DMFCs) and in making other chemicals, and so on, although it has a high toxicity in nature. In its applications, a mechanistically central question in this context is whether a metal-based regulator preferentially induces the weaker C−H bond (91.7 kcal/mol) or the stronger O−H bond (102.4 kcal/mol) (Scheme 1) in its very initial bond cleavage to convert the chemical energy into other forms, which has received extensive attention from both industry and academic units.[1]

To date, many studies on the selective cleavage C−H versus O−H of methanol by various compounds, especially transition-metal complexes (TMC) have been reported, for example, the gas-phase reaction of metal[2−5] and oxo−metal cations,[6−10] bioinspired metal compounds,[11] the environmentally benign high-valent iron−oxo species and their biomimetics,[12] etc. Greeley reported that the initial C−H scission is likely to be dominant on Pt(111).[3,5] Deng found the reaction enthalpies for the hydrogen abstraction of C−H is smaller than that of O−H, whereas the bond addition enthalpies are on the opposite trend for group 5 to group 8 TM oxides model complexes.[13] Recently, Schlangen[10,15] proposed that the activation of O−H and C−H bonds of methanol is metal-dependent and two-state-reactivity (TSR)[14] pattern might be involved. These combined experimental and theoretical studies provided deep insight mechanically; however, the mechanistic picture is still incomplete.

We recently launched a program to investigate the cleavages of methanol's C−H and O−H by TMC theoretically, to provide fundamental information for experiments on catalyst

Scheme 1. Initial Steps Considered in Methanol Oxidation

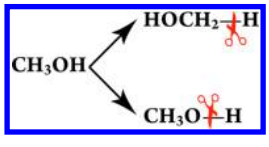

Received: June 7, 2014
Revised: July 28, 2014
Published: August 5, 2014

dx.doi.org/10.1021/jp505662x | J. Phys. Chem. A 2014, 118, 7146−7158

design and development. Metal−oxides with an $O^{\bullet-}$ oxygen radical exhibit high reactivity in hydrogen atom transfer (HAT).[16,17] As a catalyst, ferryl ($Fe^{IV}O^{2+}$), first known to be formed from the reaction of Fe(II) with ozone,[18] is of importance for evaluating the role of iron in the chemistry of the gas atmosphere. The reactions of bare FeO^{2+} with benzene, phenol, nitrobenzene, and so on, have been investigated experimentally and theoretically as well.[19−21] Further, Yoshizawa,[22−31] de Visser,[32−37] Neese,[38,39] Solomon,[40−45] and Shaik[46−54] and so on carried out extensive studies on the iron-oxo reactivities. In our previous study, it clearly showed that the catalysis of benzene hydroxylation by bare $Fe^{IV}O^{2+}$ offers a rich and complex mechanistic puzzle, hence the methanol redox reaction promoted by it can also represent a paradigmatic, challenging test case for electronic structure approaches to transition metal (TM) catalysis.

Nowadays, more and more scientists are using theoretical and computational chemistry (TCC) as a powerful tool, as a complement of experimental information, thereby to probe subtle micromechanistic details. Theory-aided experiments are becoming more and more popular, especially for chemists. The central concerns are mainly the geometry optimization, the calculations of the single-point energy (SPE), and how to deal with the solvation according to eq 1.

$$\Delta H = E_{ele} + \text{therm} + \text{solvation} + \text{D3} \quad (1)$$

where E_{ele} is the refined electronic energy via single-point energy calculations at higher level of theory based on the geometry obtained at moderate level; "therm", the thermal enthalpy correction including the zero-point energy (ZPE); "solvation", the sum of the three nonpolar continuum solvation energy corrections (cavitation, dispersion, and repulsion) by the polarized continuum method (PCM) and the electrostatic solvation energy, generally obtained by conductor-like screen model COSMO;[55] and D3, the well-known empirical dispersion correction DFT-D3.[56] In the literature, there are always mismatches between experiments and theoretical results because the theory predictions are sensitive to the methods used. Some cases show that the theoretical results are in agreements with experimental results, but for the wrong reasons.[57,58]

High-quality computations are critical to obtain meaningful predictions. Motivated by these practical questions, a thorough theoretical study on the reaction $[FeO + CH_3OH]^{2+}$ was carried out. In this article, although we have not considered the ligand effects that might play an essential role in the reactivity of the transition metal complex in condensed phases, the detailed reaction pathways were explored and considerable changes were found in the calculated energies when the theoretical calculations are improved with different methods. It is expected that the conclusion from this "simple" case can provide valuable clues for further research in understanding the C−H and O−H bond activation of alcohols on one hand, and on the other hand, from the theoretical point of view, detailed research offers new possibilities for testing the accuracy of quantum mechanical (QM) calculations, especially on highly charged TM systems with half-occupied d-blocks metals regulated multielectron transfer processes. In addition, this study provided valuable insights into the metal oxides reactivity.

2. COMPUTATIONAL DETAILS

Due to the several accessible spin states for the metal-containing active site, the reaction of methanol with FeO^{2+} has been explored on both the triplet (IS) and quintet states (HS).[21] The geometries of all structures were first optimized by employing the unrestricted B3LYP hybrid density functional (DF).[59,60] It is the most widely used DF, and it has a well documented accuracy: For molecules containing first- and second-row atoms, the errors are seldom higher than 13 kJ/mol, and for transition-metal biochemistry, the accuracy is normally within 21 kJ/mol.[61] Various basis sets def2-SVP (S), def2-TZVP (T), def2-TZVPP (TP), and def2-TZVPD (TD) were employed for all the elements for the geometry optimization.[62]

All of the above geometries were fully optimized without symmetry constraints. Harmonic vibrational frequencies were computed to verify the nature of the stationary points. Therefore, the minimum structures reported show positive eigenvalues of the Hessian matrix, whereas the transition states (TSs) have only one negative eigenvalue. Relaxed scans along the minimum energy paths (MEPs) were carried out starting from the reactant side to the product directions along the reaction coordinates (RCs) to verify the correct connections of topology. Zero-point energies (ZPE), as well as thermal correction to enthalpy at temperatures of 298.15 K and a pressure of 1 atm pressure were calculated from unscaled vibrational frequencies within the ideal gas, rigid-rotor, and harmonic oscillator approximations. All these geometry optimization and frequency calculations were carried out by Turbomole 6.3.[63]

On considering that TM systems are quite challenging for any single DFT method, BP86,[64,65] BHandHLYP,[66] and B2K-PLYP[67] methods were therefore employed to reoptimize the structures to obtain the diversities of DFT performance. The Def2-TZVP basis set was used in these calculations and carried by ORCA program.[68]

To further refine the energetics of the reaction potential energy surfaces (PESs), productive 19 DFT SPE calculations on the B3LYP/T structures were conducted with pure functionals HFS,[69] BP86,[64,65] PBE;[70] hybrid functionals with different amount of Hartree−Fock (HF) exchange TPSSh (0.10),[71] O3LYP (0.12),[72] ωB97XD (0.20),[73] X3LYP (0.22),[74] PBE0 (0.25),[75] PW1PW (0.25),[76] TPSS0 (0.25),[77] M06 (0.27),[78] PW6B95 (0.28),[79] PWPB95 (0.50),[80] BHandHLYP (0.50),[66] B2PLYP (0.53),[81] B2T-PLYP (0.60),[67] B2GP-PLYP (0.65),[82] B2K-PLYP (0.72)[67] with def2-QZVPP (QP) basis set to check the diverse prediction by different DFT functional. In addition, MP2/QP SPEs were provided as well. On the other hand, selected SPEs calculations are also performed on the BP86, BHandHLYP and B2K-PLYP optimized structures. In addition, B3LYP SPE calculations on these B3LYP optimized structures with the S, T, Q, QP, QD basis sets were performed to check the convergence of the basis set.[68] Furthermore, SPE calculations of coupled-cluster theory with single and double excitations and a noniterative perturbative triples approximation (CCSD(T))[83] were also performed in conjunction with TP basis set to calibrate the DFT energies. ORCA[68] was used for all SPE calculations.

To take into account the role of polar solvent effects, the conductor-like screen model (COSMO)[55] developed by Klamt was used and dielectric constants of 4, 36, and 78 were chosen to mimic the protein-like, biomimetic inorganic model and aqueous phases, respectively, to estimate the dielectric interactions. The COSMO calculations were carried out with ORCA. In addition, nonpolar continuum-solvation cavitation, dispersion, and repulsion energies were estimated for all

dx.doi.org/10.1021/jp505662x | J. Phys. Chem. A 2014, 118, 7146−7158

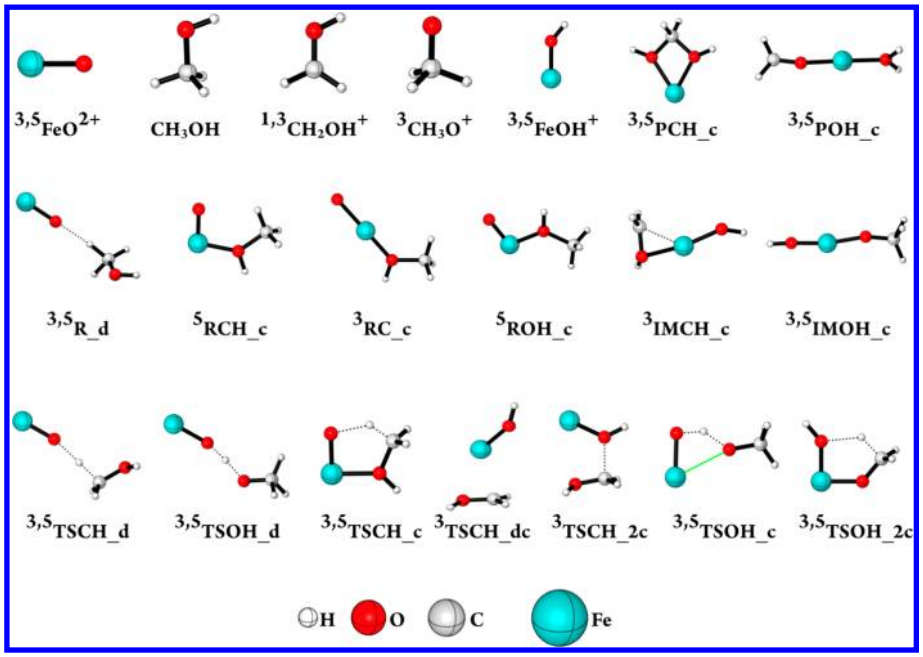

Figure 1. Structures of the various states along the reaction coordinates obtained at the DFT level of theory. Key geometry parameters are given in Table 1 and S1 (Supporting Information). The superscript m and n in ^{m,n}X represent the spin multiplicity of the species.

complexes with the polarized continuum method (PCM) as implemented in Gaussian 03 packages.[84] These calculations used the UAKS radii (united atom topological model for Kohn−Sham theory), and they are needed to obtain valid solvation energies for all reactants, as well as a balance in the dispersion energy terms for reactions in which a ligand from solution binds to or dissociates from a metal complex. The ether (ε = 4), acetonitrile (ε = 36), and water (ε = 78) solvents were used to coincide the COSMO calculations and obtain the total solvent effects.

Finally, empirical dispersion correction for all stationary points was estimated by the Grimme DFT-D3 stand-alone code.[56]

3. RESULTS AND DISCUSSION

In this section, we first show the results obtained at B3LYP/def2-TZVP level of theory and then present the comparison discussion of structures optimized at various DFs and basis sets and the SPEs calculated by different methods. Notably, in most of these channels, the high- and the intermediate-spin analogues share similar characters. Therefore, if not stated clearly, we only discuss on the quintet state cases.

3.1. Structures. The structures of the various states along the reaction coordinates obtained at the B3LYP/T level of theory are shown in Figure 1 and key parameters are listed in Table 1. In this study, we started by the separated structures[3,5] FeO^{2+} and CH_3OH in their reactant states (separated reactants, SR) and then put the educts together to locate the prereaction complexes (RC). In RC, the iron−oxo moiety and the substrate are expected to combine weakly, as we did in the study of benzene hydroxylation.[21] However, when the hydrogen of C−H or O−H is pointing toward the oxo moiety of FeO^{2+}, which resembles the classical direct hydrogen abstraction by ligated compounds Fe(IV)═O^{2+},[38,53,85] the "RC" does not exist and the two parts always departures from each other no matter how close in the starting structures. Mulliken charge analysis demonstrates that cationic FeO moiety has only one positive charge, and therefore, an electron is already shifted from substrate methanol. This can be attributed to the fact of the high FeO^{2+} oxidation potential. The equally distributed positive charges between the reactant educts generates considerable coulomb repulsion and results in the two isolated parts in mechanism 1 (M1), and mechanism 2 (M2) are over 20 Å far away with each other (Scheme 2). Because no RC involved between SRs and TSs along the reaction coordinates, these two mechanisms are named direct hydrogen transfers (DHTs), with sign "_d" in their names. Differently, three methanol ligated FeO^{2+} complexes (^{5}RCH_c, ^{5}ROH_c, and ^{3}RC_c) were found in mechanism 3 (M3), and mechanism 4 (M4), in which the oxygen of methanol coordinates to the Fe center in *cis*- or *trans*-fashion to oxo, for the high and low spin analogues, respectively. All of the elementary steps in these two mechanisms take place in concerted manners, so they are named concerted hydrogen transfers (CHTs), with sign "_c" in their names. In ^{5}RCH_c, the Fe−O_{oxo}, and Fe−O_{sub} (subscript "sub" denotes substrate methanol) distances are 1.57 and 1.85 Å, respectively; the corresponding values are quite close, 1.57 and 1.84 Å, respectively, in ^{5}ROH_c. The Fe−O_{oxo} bond is substantially shorter than those found with water ligands (0.07 Å),[19] in P450 system (0.08 Å)[50] and nonheme (up to 0.11 Å).[86,87]

Starting from R_d, the hydrogen abstractions from the methyl and hydroxyl groups show quite different features like the σ versus π pathways in HAT to iron(IV)-oxo species that were first identified first by de Visser and Solomon et al. and also recently discussed by Goldberg.[88−91] First, the methyl hydrogen transfer features a collinear Fe−O−H arrangement in both the quintet and triplet surfaces ($\angle$Fe−O−H = 162° in ^{5}TSCH_d, 176° in ^{3}TSCH_d). However, in the hydroxyl hydrogen transfer process, a bent mode rather than the collinear arrangement found in the quintet state surface is found in the triplet state surface ($\angle$Fe−O−H = 165° in 5TSOH_d, $\angle$Fe−O−H = 149° in 5TSOH_d). Second, the methyl hydrogen transfer features a typical earlier transition

dx.doi.org/10.1021/jp505662x | J. Phys. Chem. A 2014, 118, 7146−7158

Table 1. Important Distances and Angles in Various States of All the Pathways, Obtained at the B3LYP/def2-SVP (S Column), B3LYP/def2-TZVP (T), B3LYP/def2-TZVPP (TP), and B3LYP/def2-TZVPD (TD) Levels of Theory, Respectively[a]

state	S	T	TP	TD	state	S	T	TP	TD
^{5}TSCH_d					^{5}TSOH_d				
Fe−O_{xo}	1.65	1.66	1.66	1.66	Fe−O_{xo}	1.68	1.69	1.69	1.69
O_{xo}−H_t	1.51	1.52	1.53	1.53	O_{xo}−H_t	1.10	1.10	1.10	1.10
C−H_t	1.27	1.26	1.26	1.26	C−H_t	1.12	1.10	1.10	1.10
C−O_M	1.32	1.33	1.33	1.33	C−O_M	1.33	1.33	1.33	1.33
O_M−H_t	0.99	0.98	0.98	0.98	O_M−H_t	1.36	1.36	1.35	1.36
∠Fe−O_{xo}−H_t	170.8	161.7	162.7	161.6	∠Fe−O_{xo}−H_t	179.6	164.7	169.5	171.1
^{3}TSCH_d					^{3}TSOH_d				
Fe−O_{xo}	1.79	1.79	1.79	1.79	Fe−O_{xo}	1.76	1.76	1.76	1.76
O_{xo}−H_t	1.36	1.36	1.36	1.36	O_{xo}−H_t	1.19	1.19	1.20	1.20
C−H_t	1.35	1.37	1.37	1.36	C−H_t	1.11	1.10	1.10	1.10
C−O_M	1.31	1.33	1.31	1.31	C−O_M	1.33	1.34	1.34	1.34
O_M−H_t	0.98	0.98	0.98	0.98	O_M−H_t	1.23	1.22	1.21	1.22
∠Fe−O_{xo}−H_t	177.6	176.3	174.7	174.8	∠Fe−O_{xo}−H_t	152.7	149.4	149.5	148.7
^{5}TSCH_c					^{5}TSOH_c[b]				
Fe−O_{xo}	1.64	1.64	1.64	1.64	Fe−O_{xo}	1.87			
O_{xo}−H_t	1.85	1.79	1.77	1.80	O_{xo}−H_t	1.17			
C−H_t	1.17	1.17	1.17	1.17	C−H_t	1.10			
C−O_M	1.41	1.42	1.42	1.42	C−O_M	1.34			
O_M−H_t	0.99	0.98	0.98	0.99	O_M−H_t	1.30			
Fe−O_M	2.11	2.09	2.08	2.09	Fe−O_M	2.66			
∠Fe−O_{xo}−H_t	110.8	110.1	110.1	109.8	∠Fe−O_{xo}−H_t	98.4			
^{3}TSCH_c					^{3}TSOH_c				
Fe−O_{xo}	2.01	1.98	1.97	1.97	Fe−O_{xo}	1.88	1.87	1.87	1.87
O_{xo}−H_t	1.39	1.41	1.44	1.43	O_{xo}−H_t	1.17	1.16	1.16	1.16
C−H_t	1.26	1.25	1.24	1.24	C−H_t	1.10	1.09	1.09	1.09
C−O_M	1.44	1.44	1.44	1.43	C−O_M	1.34	1.35	1.35	1.35
O_M−H_t	0.99	0.98	0.98	0.98	O_M−H_t	1.32	1.33	1.34	1.34
Fe−O_M	2.01	2.00	2.01	2.01	Fe−O_M	2.61	2.58	2.59	2.58
∠Fe−O_{xo}−H_t	100.4	99.4	97.6	99.3	∠Fe−O_{xo}−H_t	96.1	95.36	95.16	95.29
^{3}IMCH_c					^{5}IMOH_c				
Fe−O_{xo}	1.85	1.84	1.84	1.85	Fe−O_{xo}	1.70	1.69	1.69	1.69
O_{xo}−H_t	1.00	0.98	0.98	0.99	O_{xo}−H_t	0.99	0.98	0.98	0.98
O_M−H_t	0.99	0.99	0.99	0.99	Fe−O_M	1.84	1.84	1.83	1.83
∠Fe−Oxo−H_t	159.8	146.7	145.7	143.8	∠Fe−O_{xo}−H_t	178.5	177.1	177.5	177.4
^{3}TSCH_2c					^{3}IMOH_c				
Fe−O_{xo}	1.83	1.83	1.84	1.84	Fe−O_{xo}	1.85	1.85	1.84	1.85
O_{xo}−H_t	0.99	0.98	0.98	0.98	O_{xo}−H_t	1.00	0.99	0.99	0.99
C−O_{xo}	1.82	1.80	1.80	1.79	Fe−O_M	1.81	1.81	1.81	1.81
O_M−H_t	0.98	0.98	0.98	0.98	∠Fe−O_{xo}−H_t	178.0	149.5	149.5	146.4
∠Fe−O_{xo}−H_t	125.5	126.5	125.8	124.9					
^{5}PCH_c					^{5}POH_c				
Fe−O_{xo}	2.01	2.00	2.00	2.00	Fe−O_{xo}	1.95	1.95	1.94	1.94
O_{xo}−H_t	0.98	0.98	0.98	0.98	O_{xo}−H_t	0.98	0.98	0.98	0.98
C−O_M	1.44	1.44	1.44	1.44	Fe−O_M	1.88	1.87	1.87	1.87
O_M−H_t	0.98	0.98	0.98	0.98	C−O_M	1.24	1.24	1.24	1.23
∠Fe−O_{xo}−C	100.1	100.1	100.1	100.1					
^{3}PCH_c					^{3}POH_c				
Fe−O_{xo}	1.94	1.94	1.95	1.95	Fe−O_{xo}	1.93	1.94	1.92	1.93
O_{xo}−H_t	0.98	0.98	0.98	0.98	O_{xo}−H_t	0.98	0.98	0.98	0.98
C−O_M	1.45	1.45	1.45	1.45	Fe−O_M	1.87	1.86	1.86	1.86
O_M−H_t	0.98	0.99	0.98	0.98	C−O_M	1.23	1.23	1.23	1.23
∠Fe−O_{xo}−C	99.0	98.7	98.5	98.5					
^{3}TSCH_dc[c]									
Fe−O_{xo}	1.78	1.79							
O_{xo}−H_t	0.99	0.98							
C−O_M	1.29	1.29							
O_M−H_t	0.98	0.99							
Fe−C	2.45	2.44							

dx.doi.org/10.1021/jp505662x | J. Phys. Chem. A 2014, 118, 7146−7158

Table 1. continued

state	S	T	TP	TD	state	S	T	TP	TD
∠Fe−C−O_M	79.4	79.6							

[a] O_{xo} is the oxygen atom of the Fe═O moiety, whereas O_M is the oxygen atom in the methanol part. H_t is the transferred hydrogen atom during the reaction. Distance, angstrom. Angle, degree. [b] ^{5}TSOH_c can only be located at def2-SVP level. [c] ^{3}TSCH_dc cannot be found by B3LYP with any basis set; it is the top point on the relaxed MEP scan.

Scheme 2. Reaction Pathways Considered in This Study

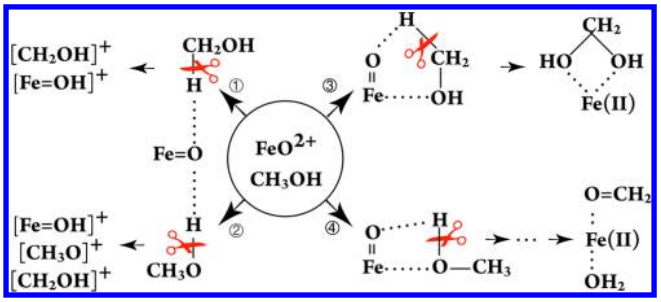

state (TS) whereas the hydroxyl hydrogen transfer has a very late TS feature (see structural parameters shown in Table 1). As shown in Table 1, ^{5}TSCH_d has a 1.26 Å broken C−H and 1.52 Å forming O−H bonds, whereas the corresponding distances are 1.36 and 1.10 Å in ^{5}TSOH_d, respectively. These sharp contrasts on forming/broken bonds in these TSs indicates that the C−H bond is expected to be easily cleaved whereas the O−H bond is sluggish in methanol when they are regulated by Fe(IV)O^{2+}. This is also confirmed from energetic analysis (*infra*). Subsequently, after the hydrogen transfer TSs, the metal−oxo moiety results in $FeOH^+$ by obtaining a hydrogen and the substrate gives rise to hydroxymethyl CH_2OH^+ in M1 (PCH_d) and M2 (POH_d) and methoxy CH_3O^+ in M2 with losing that hydrogen. It is worth noting here that no singlet methoxy cation exists and only triplet CH_3O^+ was located in our calculations.[92]

Starting from RCs (^{5}RCH_c, ^{5}ROH_c, and ^{3}RC_c), the hydrogen transfers take place via five-centered (TSCH_c) TS in M3 and four-centered (TSOH_c) TS in M4 (Scheme 2). Structurally, the ∠Fe−O−H angles in these two TSs are bent severely as shown in Figure 1. In M3, the substrate methanol uses the hydroxyl to ligate with iron atom and the methyl C−H to attack the oxo radical, forming five-centered TSs TSCH_c. The TSs for C−H bond cleavage appear very early on both quintet and triplet PESs: 1.17 Å C−H and 1.79 Å O−H bond distances, whereas the TS for O−H is relative late with 1.30 and 1.17 Å for the two O−H bond, respectively. We should note here that the ^{5}TSOH_c cannot be located at B3LYP level with basis set larger than def2-SVP. From the structure inspection, we can also infer the relative reactivity in these pathways. For example, we may tell that although the TSOH_c in M3 is relatively late compared with TSCH_c in C−H activation, but still a little bit more reactive than that in the direct mechanism M2. Likewise, we may also speculate that the less competitive

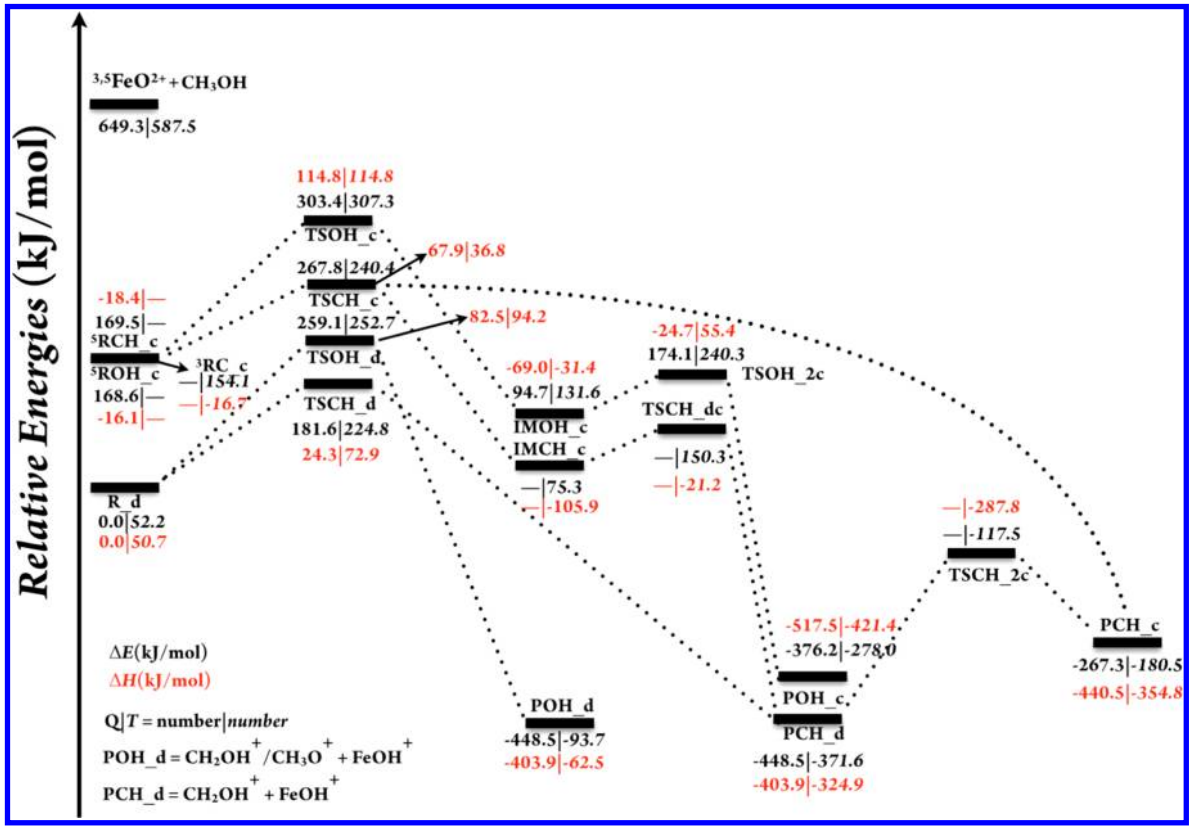

Figure 2. CCSD(T)/TP//B3LYP/T potential energy surfaces for the title reaction. Δ*E* values are given in black, and Δ*H* values with solvent effect at ε = 4 are given in red. Values before and after "|" correspond to the quintet and triplet values. Unit, kJ/mol.

dx.doi.org/10.1021/jp505662x | J. Phys. Chem. A 2014, 118, 7146−7158

of M4 compared with M3 may also arise from the large unfavorable structure reorganization because the coordination of hydroxyl to iron changes from 2.09 to2.66 Å in ^{5}TSCH_c and ^{5}TSOH_c, respectively.

After the initial hydrogen transfers, the quintet and triplet pathways are entirely different in M3. The "O rebound"[93] step is barrierless in the quintet ^{5}TSCH_c → ^{5}PCH_c surface, whereas a multistep process is encountered in the triplet surface: ^{3}TSCH_c → ^{3}IMCH_c → ^{3}TSCH_dc → ^{3}TSCH_2c → ^{3}PCH_c. We should mention here that the true TS for the cationic hydroxymethyl dissociation from $FeOH^+$ is hard to be located due to the very flat energy surface in this region, and the ^{3}TSCH_dc reported here is a top point on a very elaborative relaxed MEP scan. The barrierless rebound step implies that the C−H bond activation could proceed without the oxygen rebound step, which gives important clues for effective catalyst design.[94] On the other hand, the subsequent steps in M4 are quite similar: it first goes to intermediate ^{3,5}IMOH_c, in which the OH group and the CH_3O part are in *trans* fashion (Figure 1), and then the C−H bond cleavage takes place, and a second hydrogen transfer to the OH group via TSOH_2c, giving rise to water and formaldehyde finally. The geometry inspection indicates that the TSOH_2c are early TSs on both PESs.

By inspection of Table 1, one can see that the geometry parameters predicted with basis sets def2-TZVP, def2-TZVPP, and def2-TZVPD are highly consistent: (1) for bond distances, the deviations are less than 0.01 Å for most cases, only with a few exceptions; (2) for angles, the deviations are less than 6°. However, obvious deviations should not be neglectful between the results of SVP and triple-ζ basis sets: (1) for bond distances, 0.01−0.02 Å offsets are dominant, and it even goes to 0.08 Å in ^{5}TSCH_c; (2) the angles can departure over 10°. The extreme case is ^{5}TSOH_c: It can only be located at the B3LYP/S level; when larger basis sets, for instance def2-TZVP, are used, it results in the unbinding between the hydroxyl and iron center. We attribute the existence of ^{5}TSOH_c at B3LYP/S to the overstabilization of the small basis set to a given geometry. These deviations might be amplified further when SPE corrections protocol at higher level are used, because sizable displacement of the TS position is unavoidable.[57,95] Therefore, at the DFT level triple-ζ basis sets are highly recommended for similar systems to obtain reliable structure parameters.[62]

Table S1 (Supporting Information) lists the important geometry parameters obtained by BP86, BHandHLYP, and B2K-PLYP, respectively, with def2-TZVP basis sets. Briefly, one can find that (1) for all the stationary points located, the Fe−O bond distances are most sensitive to the density functionals, and the max deviations are over 0.60 Å even in the reactants, (2) all four methods give very similar structures for the products, and the deviations are less than 0.03 Å, and (3) the structures given by BP86 are close to that of B3LYP and the those of BHandHLYP are close to that of B2K-PLYP, in general, but for the Fe−O bond and the C−H/C−H bond involved in the transition states, no two methods are in good agreement. Therefore, it is not meaningful to discuss which DFT method could give the accurate prediction of the geometries, especially for transition structures.

3.2. Energies. *3.2.1. Potential Energy Surface.* The CCSD(T)/TP//B3LYP/T gas-phase potential energy surfaces of various reaction pathways are shown in Figure 2. We confine our discussion in this section by using the gas-phase energetics without considering the correction terms in eq 1, for example, the solvation (*infra*). It can be seen that the quintet RCs, ^{5}ROH_c, and ^{5}RCH_c, being very close in energy, lie ∼169 kJ/mol above the reactants R_d, which lies 587 kJ/mol below the isolated $^3FeO^{2+}$ and methanol. This situation is because one electron has been transferred from methanol to FeO^{2+} in R_d, which weakens the C/O−H bond strength in methanol. So, the pathways starting from R_d can be regarded as the reaction of $Fe(III)O^+$ with the CH_3OH^+ cation radical (M1 and M2); however, these channels from methanol ligated complexes can be regarded as the extreme simple model of $Fe(IV)O^{2+}$ with its ligand CH_3OH (M3 and M4). Notably, the gas-phase calculations herein resulted in a long-rang electron transfer and the iron(IV)−oxo converting to an iron(III)−oxo. We also tried to optimize the structures by the implicit COSMO solvent model as we did before;[85] however, the self-interaction error (SIE)[96] cannot be avoided. We argued this problem in a recent work,[85] and research continues in our group.

As shown in Figure 2, the DHTs starting from methyl in M1 need to overcome 182/225 kJ/mol (quintet/triplet, *infra*) barriers (^{5,3}TSCH_d) to reach PCH_d with −449/−372 kJ/mol heat released finally. Comparatively speaking, the DHT pathways from hydroxyl in M2 have lower reactivity because 77/28 kJ/mol higher activation barriers are encountered. Interestingly, the M2 pathways share $FeOH^+$ and CH_2OH^+ products with the M1 ones, which is −448 kJ/mol more stable than R_d. In addition, $^3CH_3O^+$ cation can also be generated in M2.

In general, the positive-charged metal−oxides have high reactivity toward C−H bond activation.[17] FeO^+ exhibits high reactivity in the conversion of methanol to formaldehyde in the gas phase, for instance.[97,98] On the other hand, the gas-phase reaction should be more reactive than the condensed phase because the solvent screens/reduces the electrostatic interactions. Small neutral iron oxide clusters oxidize methanol, and $[FeO(H_2O)_5]^{2+}$ has also been studied.[19] Among these reactions, the rate-controlling barriers are relatively low. Therefore, for the highly oxidized $[FeO + CH_3OH]^{2+}$ system, the channels in M1 and M2 are of course expected have very high reactivity.

The CHT mechanism starts from the binding complexes RCs. The methyl H can transfer to the oxo radical by surmounting 98/86 kJ/mol barriers. Subsequently, the quintet state pathways can lead to the product directly with −267 kJ/mol energy released or go though by multistep process ^{3}TSCH_c → ^{3}IMCH_c → ^{3}TSCH_dc → ^{3}TSCH_2c → ^{3}PCH_c. In the whole processes, the rate-controlling step is the first hydrogen transfer. In addition, a junction between the direct and the concerted mechanisms happens at the PCH_d point, making the reaction pathways diverse.

Another two pathways are the concerted hydroxyl H transfers, in which 134/153 kJ/mol heats are required for the H transfers from O−H to take place in the very beginning. The intermediates IMOH_c are located 77/22 kJ/mol lower than the RCs. To accomplish the remaining steps, the reaction follows a second hydrogen transfer from methyl to hydroxyl, in which 79/108 kJ/mol barriers are encountered before arriving at the product POH_c with −376/−278 kJ/mol heat released.

To sum up, we can find the C−H bond cleavage is dominant and the O−H activation only plays a minor role on the PESs. Second, the DHT is more feasible than the CHT because of the

dx.doi.org/10.1021/jp505662x | J. Phys. Chem. A 2014, 118, 7146−7158

relative stability of these pathways. All in all, the DHT starting from the methyl position should be the most practical channel.

3.2.2. Mean Absolute Deviation. In Table S2 (Supporting Information), the deviations of various relative energies of all states compared to the CCSD(T)/TP//B3LYP/T results are given. Also, the mean absolute deviations (MADs) disregarding the ^{5}R_d state are given separately: products-only, MAD-P; all transition states-only, MAD-TS; all states, MAD-All. The MADs are plotted in Figure 3 and S1 (Supporting Information).

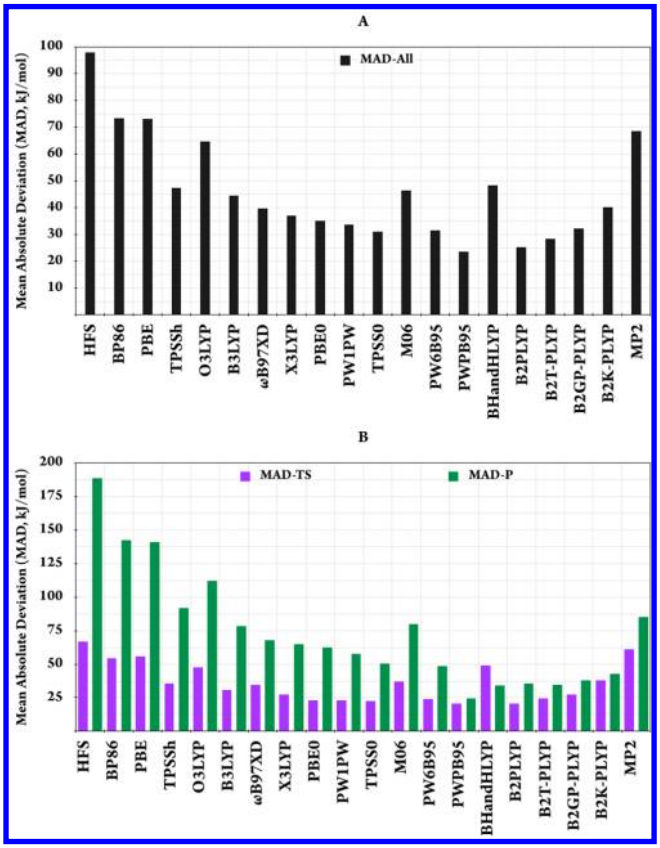

Figure 3. Mean absolute deviations (MADs) of different methods according to CCSD(T)/TP//B3LYP/T level of theory: A, MAD-All (black); B, MAD-P (green) and MAD-TS (grape). Pure functionals, hybrid functionals with the amount of HF exchange from 0.10 to 0.72 HF exchange, MP2 are from left to right. Unit, kJ/mol.

As shown in Figure 3A, the all-states MAD are in the range between 24 and 98 kJ/mol; the HFS functional has the largest MAD and the PWPB95 the smallest value. Generally, the MAD changes as the fraction of HF exchange. As the fraction increases from 0 to 0.5, the MAD decreases; however, the MAD increases as the fraction does from 0.5 to 0.72, except TPSSh, M06, and BHandHLYP. The MADs become strikingly larger (over 50 kJ/mol) at the theory level of pure DFs, BHandHLYP, and MP2 methods. For different states, the absolute maximum error between different methods can reach to 268 kJ/mol (^{3}TSCH_2c, HFS) for TSs and 251 kJ/mol (^{3}PCH_c, HFS) for products. Notably, the overall MAD of HFS is even over 98 kJ/mol. Furthermore, we see that the much more expensive MP2 generally shows larger errors than most of the density functionals.[99−103] The large functional effect is not very surprising, and therefore, high-level methods are highly desirable if very accurate numbers are required.[57]

The MADs of barrier height and the reaction energy prediction are shown in Figure 3B. Clearly, the transition state calculations are not so sensitive to density functionals, compared with that of products. The best density functionals tested in this study for barrier heights are B2PLYP and PWPB95, only having 21 kJ/mol MAD. Also, PWPB95 is the best method for reaction energy calculations, which has 24 kJ/mol MAD (Table S2, Supporting Information), indicating the reaction energy prediction is challenging for DFT methods. From Table S2, we see that the MADs become larger when the state of species becomes far from the state ^{5}R_d, generally. This is quite expected, because similar effects have been observed before for energy differences between different spin states,[104] as well as between different oxidation states of transition metals.[57,105,106] This also reflects that the Fe's oxidation state has been changed from SR to P gradually, something that is frequently problematic to describe by the DFs, giving a strong correlation on the HF exchange in the DFs.[57,105−107] In addition, this also illustrates the danger of accepting a result without checking that the calculations are converged. This conclusion is very useful for SPE calculations if one wants to obtain reliable results, especially for the *de novo* design of catalysts research. However, for practical theoretical screening, high-level theory methods, such as the gold-standard CCSD(T) and CASSCF/CASPT2 for multireference configuration interaction (MRCI), are not possible for large scale applications because of not only the very demanding on computer resource but also the preparation of the calculation much more difficult for the users.[57]

To verify structural effects on the relative energies, we also performed SPE calculations on the structures optimized by BP86, BHandHLYP, and B2K-PLYP, respectively, with the def2-TZVP basis set. Table S3 (Supporting Information) lists the relative energies at various levels of theory. One can find that there is no obvious deviation for relative energies of reaction states calculated by one method but using geometry obtained by a different method; however, outstanding deviations are observed for the relative energies calculated by different methods but with the same geometry (Table S3, Supporting Information)! For example, the largest deviation comes up to 214 kJ/mol for ^{3}RCH_c, although its structures calculated at BP/TP//B2K-PLYP/T and B2K-PLYP/TP//B2K-PLYP/T, respectively, are very similar. Table 2 gives the CCSD(T) relative energies based on the structural obtained from the four density functionals. One can find that (i) only for ^{3}RCH_c, ^{5}TSOH_c, and ^{3}IMOH_c, CCSD(T) gives over 100 kJ/mol deviations, (ii) the BP86 structures always result in large deviations compared with those of the other three methods, and (iii) the relative energies agree with each other in general, with only a few exceptions. Therefore, we can make the conclusion that the structural factor plays a minor role in the SPE calculations.

3.2.3. Thermal, Solvation, and DFT-D3 Corrections. Briefly, the enthalpy thermal corrections (column "therm" in Table 3) shows that the correction lowers the late TSs of hydrogen transfer (HT) from O−H by −16 to −20 kJ/mol, in contrast to that of HT from C−H,+2 to −8 kJ/mol. This is expected to reduce the relative rate-limiting barriers $\Delta\Delta H$ ($\Delta\Delta H = \Delta H_{(O-H)} - \Delta H_{(C-H)}$) in these reaction pathways so that to increase the relative reactivity toward O−H bond cleavage.

The solvent plays quite important and different roles in these pathways according to our results. As shown in columns ε4, ε36, and ε78 in Table 3, we can draw the following conclusions:

dx.doi.org/10.1021/jp505662x | J. Phys. Chem. A 2014, 118, 7146−7158

Table 2. Relative Energies (Δ, kJ/mol) for the Various States Calculated at the CCSD(T)/TP Level of Theory

state	CCSD(T)-BP[a]	CCSD(T)-B3[b]	CCSD(T)-BH[c]	CCSD(T)-B2K[d]
^{5}RC_d	0.0	0.0	0.0	0.0
^{3}RC_d	57.2	52.2	23.8	38.3
^{5}TSCH_d	171.4	181.6	168.2	176.3
^{5}TSOH_d	266.7	259.1	281.7	246.4
^{3}TSCH_d	241.8	224.8	221.5	257.3
^{3}TSOH_d	269.7	252.7	245.9	253.4
$^5FeOH^+ + {}^1CH_2OH^+$	−446.9	−448.5	−478.4	−465.8
$^3FeOH^+ + {}^1CH_2OH^+$	−368.8	−371.6	−401.1	−386.9
$^5FeOH^+ + {}^3CH_3O^+$	−91.7	−93.7	−125.3	−111.1
^{5}RCH_c	173.8	169.5	174.2	186.1
^{3}RCH_c	252.5	154.1	119.9	132.0
^{5}TSCH_c	250.1	267.8	228.6	237.9
^{3}TSCH_c	272.6	240.4	304.6	218.8
^{3}IMCH_c	105.3	75.3	32.8	45.3
^{3}TSCH_dc	87.2	150.3	117.3	132.2
^{3}TSCH_2c	−93.5	−117.5	−118.1	−131.0
^{5}PCH_c	−266.1	−267.3	−297.9	−284.7
^{3}PCH_c	−180.3	−180.5	−214.9	−200.0
^{5}ROH_c	172.2	168.6	175.3	186.1
^{5}TSOH_c	368.6	303.4	266.7	281.0
^{3}TSOH_c	364.3	307.3	334.3	355.5
^{5}IMOH_c	124.2	94.7	103.6	118.7
^{3}IMOH_c	205.7	131.6	93.2	107.7
^{5}TSOH_2c	176.1	174.1	182.3	199.8
^{3}TSOH_2c	251.0	240.3	187.9	202.4
^{5}POH_c	−374.7	−376.2	−406.6	−394.0
^{3}POH_c	−274.4	−278.0	−303.7	−321.7

[a]CCSD(T)/TP//BP86/T. [b]CCSD(T)/TP//B3LYP/T. [c]CCSD(T)/TP//BHandHLYP/T. [d]CCSD(T)/TP//B2K-PLYP/T.

(1) as the dielectric constant of the solvent increases, the transition states in the direct hydrogen transfer in M1 and M2 can be lowered up to 200 kJ/mol; however, the opposite trend is observed in the concerted mechanisms of M3 and M4; (2) in the directed pathways, a larger epsilon (ε) solvent stabilizes the TSs in M1 and M3 much more, whereas that TSs are more stable under a smaller ε solvent in M3 and M4; (3) a larger ε reduces the relative barrier height $\Delta\Delta H$ ($\Delta\Delta H = \Delta H_{(TSOH\_d)} - \Delta H_{(TSCH\_d)}$) by −7 to −19 kJ/mol in direct mechanisms, therefore increasing the competitiveness of the O−H activation; however, the O−H bond activation feasibility would be reduced by 29−42 kJ/mol in the concerted mechanisms; (4) the results of ε36 and ε78 are very close, so a solvent dielectric constant larger than 36 does not affect the result much more. The solvation ε = 4 corrected PES are thus shown in Figure 2. We should mention that in a real solvation process the bounded ligands of the iron(IV)−oxo species may be dissolved by the solvent molecules, which results in ligand positions were filled by the solvent molecules. This might affect the reactivities of the iron(IV)−oxo species.

The B3LYP-D3 correction was also listed in the last column of Table 3. It can be seen that in the direct HAT mechanisms, the D3 correction lowers the barriers by 6−7 kJ/mol. However, in the concerted mechanism hydrogen transfer in M3, it only

Table 3. Thermal, Solvation (ε4, ε36, ε78), and B3LYP-D3 (D3) Corrections in Eq 1 (Unit, kJ/mol)

state	therm	ε4	ε36	ε78	D3
^{5}RC_d	0.0	0.0	0.0	0.0	0.0
^{3}RC_d	−2.9	1.4	3.5	153.0	0.0
^{5}TSCH_d	−7.6	−149.8	−211.7	−217.6	−6.8
^{5}TSOH_d	−20.2	−156.4	−230.8	−236.2	−6.3
^{3}TSCH_d	−2.7	−149.2	−212.1	−218.0	−7.0
^{3}TSOH_d	−19.6	−138.9	−203.5	−208.3	−6.6
$^5FeOH^+ + {}^1CH_2OH^+$	5.0	39.5	61.3	61.8	−1.6
$^3FeOH^+ + {}^1CH_2OH^+$	4.5	42.2	65.2	65.8	−1.3
$^5FeOH^+ + {}^3CH_3O^+$	−14.2	45.4	68.3	61.7	−1.4
^{5}RCH_c	12.3	−200.3	−285.1	−291.7	−11.2
^{3}RC_c	9.0	−179.8	−255.7	−261.3	−8.9
^{5}TSCH_c	1.6	−201.5	−285.9	−292.9	−12.5
^{3}TSCH_c	−4.5	−199.1	−280.2	−288.0	−12.2
^{3}IMCH_c	3.1	−184.3	−258.1	−265.1	−12.7
^{3}TSCH_dc	8.5	−179.9	−253.3	−260.2	−11.5
^{3}TSCH_2c	16.5	−186.8	−261.5	−269.0	−11.4
^{5}PCH_c	21.3	−194.6	−270.8	−278.8	−12.7
^{3}PCH_c	21.2	−195.5	−271.8	−279.9	−13.1
^{5}ROH_c	12.3	−197.0	−280.0	−286.3	−10.4
^{5}TSOH_c	−16.3	−172.3	−245.8	−251.0	−5.5
^{3}TSOH_c	−16.7	−175.8	−250.9	−256.2	−5.4
^{5}IMOH_c	−4.9	−158.8	−223.1	−228.0	−6.5
^{3}IMOH_c	−9.3	−153.7	−215.9	−220.6	−6.6
^{5}TSOH_2c	−8.4	−190.5	−267.0	−274.5	−11.0
^{3}TSOH_2c	−9.3	−175.6	−246.1	−251.8	−10.2
^{5}POH_c	9.3	−150.5	−209.6	−215.2	−7.7
^{3}POH_c	8.7	−152.1	−212.7	−218.4	−7.7

results in 1 kJ/mol barrier decreasing and can thus be neglected. The correction can also lead to enlarge of the barrier by 5 kJ/mol. On considering the low cost of D3 calculation, the dispersion correction is high recommended.

3.3. Electronic Structure Analysis. Detailed electronic structure analysis can provide deep insight for interpreting the reactivity of inherent nature of the iron−oxo compounds.[21,38,39,85] The rate-limiting steps of all the possible channels correspond to the first hydrogen transfer transition states as shown in Figure 2. We therefore confine our discussion on the electron evolution of the hydrogen transfer in the very initial steps.

Figure 4 and Figure 2S (Supporting Information) shows the schematic frontier molecular orbitals (FMOs) of the critical points along the possible reaction pathways. As shown in Figure 4A, for the quintet M1 of ^{5}R_d, the five unpaired spin-up (α) electrons on Fe d-block MO indicates the iron center is in the high spin (HS) state, and the corresponding antiferromagnetic (AF) spin-down (β) electron locates on the σ^*(C−O) MO. This clearly shows that one α-electron has been transferred from C−O location to Fe d_{z^2} orbital. The ^{5}TSCH_d electron configuration (EC) maintains that of ^{5}R_d. In the following step to ^{5}PCH_d, a second electron is shifted to the iron−oxo moiety as the proton transfers, indicating it is of course a classical hydrogen atom transfer (HAT). This electron evolution process is very similar for the quintet state pathway of M2 (Supporting Information).

The EC of ^{3}R_d in triplet M1 also shows a HS iron center (S_{Fe} = 2) (Figure 4B). Compared with the traditional triplet iron center (S_{Fe} = 1),[85] the iron−oxo moiety does have two

dx.doi.org/10.1021/jp505662x | J. Phys. Chem. A 2014, 118, 7146−7158

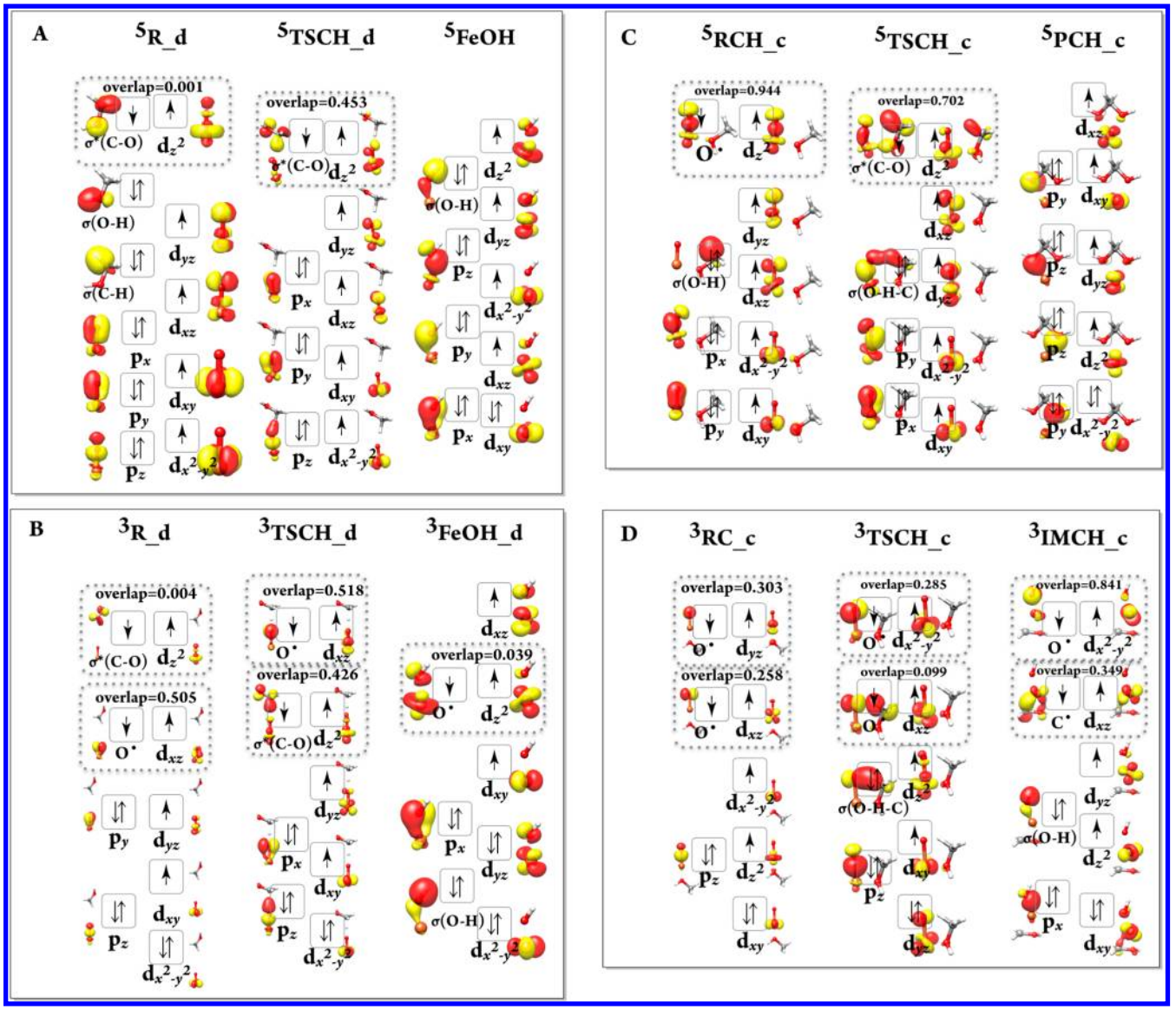

Figure 4. Schematic FMO diagrams. The insert overlap value represents the overlap of these two MOs. (A) Direct hydrogen transfer in the quintet state of **M1**. (B) Direct hydrogen transfer in the triplet state of **M1**. (C) Concerted hydrogen transfer in the quintet state of **M3**. (D) Concerted hydrogen transfer in the triplet state of **M3**.

extra electrons, which come from oxo and σ(C−O) of methanol, respectively. Subsequently, another electron from σ(C−H) transfers to d_{yz} MO, and the σ^*(C−O) electron couples with the remaining electron on C$^\bullet$ radical, generating the C−O bond again. Thus, it can be seen this whole process should be regarded as a two-electron coupled hydrogen atom transfer. One can also see that the EC of ^{3}TSOH_d in the triplet M2 pathways has great similarity with that of ^{3}TSCH_d. The only difference is C−H or O−H involved in the FMO (Figure 2S, Supporting Information).

In the HS concerted mechanism M3, an electron on O Pz migrates to Fe d_{z^2} during the initial step (^{5}RCH_c), giving rise to an O$^\bullet$ radical (Figure 4C). From ^{5}RCH_c to ^{5}TSCH_c, an α-electron on σ(C−O) is shifted to O Pz, resulting in the formation of σ(C−H−O). During the process of ^{5}TSCH_c to ^{5}PCH_c, an electron on σ(C−H) is shifted to the iron nonbonding orbital, and the remaining electron of the C$^\bullet$ radical couples with the singly electron on σ^*(C−O), re-forming C−O bond. However, the electron evolution is different in HS of M4 (Figure 2S, Supporting Information). Being a late TS ^{5}TSOH_c, a β electron on σ(C−O) is shifted to Fe d_{xy}. On the other hand, the O$^\bullet$ radical accepts the hydrogen atom from C−H, giving rise to a σ(O−H). In addition, a σ^*(C−O) is given rise after the hydrogen atom transfer reaction; the β-electron on the doubly occupied electron on d_{xy} is shifted back to O$^\bullet$ radical, by generating O p_y.

In the intermediate spin (IS) concerted mechanism M3, the ^{3}RC_c forming also involved 2e transfer as that found in ^{3}R_d, but from a different location, as shown in Figure 4D. With ligand coordination, the oxo is a biradical, resulting in the enhancement of its reactivity toward C−H activation, in agreement with previous observation in Figure 4 of ref 108. As shown in Figure 2, the rate-controlling TSs of HS is 43 kJ/mol lower than that of IS in M1, whereas the situation of HS-IS are upside down in M3: the IS channel has lower barrier (240 kJ/mol) than HS does (260 kJ/mol)! On considering that the terminal O$^\bullet$ radical directed catalysts for methane C−H bond activation in Schwarz group, this finding is of course

dx.doi.org/10.1021/jp505662x | J. Phys. Chem. A 2014, 118, 7146−7158

meaningful.[17] During the EC developments from ^{3}RC_c → ^{3}TSCH_c → ^{3}IMCH_c, one can find that different pathways are employed for proton and electrons, so the HAT here is better regarded as proton coupled electron transfer (PCET).[109] In addition, in IS channel of M4 from ^{3}RC_c to ^{3}TSOH_c, it is the interaction between the O$^\bullet$ radical and the σ(C−H), forming σ(O−H) finally. As a result, the newly formed $[O_{(CH3O)}]^\bullet$ radical leads to σ^*(C−O). Furthermore, in the IS of M3 and M4, the formal electrons on the iron center remain unchanged, one paired and four singly spin-up, coupled with two spin-down electrons from substrate moiety, as shown in Figure 2S (Supporting Information).

4. CONCLUSION

In the present study, we performed a high-level computational study on methanol C−H and O−H bond cleavages by bare $[Fe^{IV}O]^{2+}$. Mechanistically, both direct and concerted hydrogen transfers (DHT and CHT) pathways were considered for the title reaction. The calculations disclosed that the C−H cleavage is dominant and the DHT from methyl is calculated to be the most feasible channel. The electronic structure analysis revealed the proton and electron transfer coupling behavior along the reaction coordinates. Furthermore, the correlation between structural optimization and density functional methods (as well as basis sets), solvent effect, and CCSD(T) benchmark were also explored. Overall, we can draw the following conclusions:

(i) Good basis set convergence for structural optimization can be obtained at DFT-B3LYP/TZ level;
(ii) Structural optimization by different density functional methods shows it is not meaningful to discuss which DFT method could give the accurate prediction of the geometries, especially for transition structures;
(iii) The structural factor plays a minor role in the single point energy (SPE) calculations and reaction energy prediction is quite challenging for DFT methods;
(iv) The average of mean absolute deviations (MADs) in the relative energies from SPE at different levels of theory results in the diverse of DFT predictions and higher level methods, for instance CCSD(T), are highly recommended;
(v) The MADs reflect the problematic description of the DFs when dealing with metal oxidation state change, giving a strong correlation on the HF exchange in the DFs;
(vi) The solvent plays distinct roles in different pathways of these C−H and O−H bond activations during this catalytic process.

In relating this gas-phase bare FeO^{2+} with methanol reaction to condensed-phase process, it is important to realize that model will not equal the ligand saturated metal−oxide catalysis. The relationship between the gas and condensed phase is more elusive, but this theoretical scrutiny expects that the intrinsic gas-phase reaction mechanisms are useful starting points for comparison, analysis, and prediction of condensed-phase insights. The conclusion of this computational survey should be therefore of great values for transition metal systems research.

■ ASSOCIATED CONTENT

Supporting Information

The mean absolute deviations of the B3LYP method with different basis sets, schematic FMO diagrams, tables for the structural parameters, the MADs, relative energies, and coordinates of all the states at B3LYP/def2-TZVP level of theory. This material is available free of charge via the Internet at http://pubs.acs.org."

■ AUTHOR INFORMATION

Corresponding Author

*J. Li. E-mail: Jilai@jlu.edu.cn.

Present Address

[§]Institut für Chemie, Technische Universität Berlin, Straße des 17. Juni 115, 10623 Berlin, Germany.

Author Contributions

[‖]These authors contributed equally.

Notes

The authors declare no competing financial interest.

■ ACKNOWLEDGMENTS

This project was supported by the National Basic Research Program of China (973 Program, 2012CB932800), and the National Natural Science Foundation of China (No. 21103064).

■ REFERENCES

(1) Schwarz, H. Chemistry with Methane: Concepts Rather Than Recipes. *Angew. Chem., Int. Ed.* **2011**, *50*, 10096−10115.
(2) Desai, S. K.; Neurock, M.; Kourtakis, K. A Periodic Density Functional Theory Study of the Dehydrogenation of Methanol over Pt(111). *J. Phys. Chem. B* **2002**, *106*, 2559−2568.
(3) Greeley, J.; Mavrikakis, M. A First-Principles Study of Methanol Decomposition on Pt(111). *J. Am. Chem. Soc.* **2002**, *124*, 7193−7201.
(4) Jiang, R. B.; Guo, W. Y.; Li, M.; Fu, D. L.; Shan, H. H. Density Functional Investigation of Methanol Dehydrogenation on Pd(111). *J. Phys. Chem. C* **2009**, *113*, 4188−4197.
(5) Greeley, J.; Mavrikakis, M. Competitive Paths for Methanol Decomposition on Pt(111). *J. Am. Chem. Soc.* **2004**, *126*, 3910−3919.
(6) Blum, O.; Stöckigt, D.; Schröder, D.; Schwarz, H. O−H Bond Activation in the Gas Phase: The Reactions of Water and Methanol with $[FeCH_3]^+$. *Angew. Chem., Int. Ed.* **1992**, *31*, 603−604.
(7) Engeser, M.; Schroder, D.; Schwarz, H. Gas-Phase Dehydrogenation of Methanol with Mononuclear Vanadium-Oxide Cations. *Chem.—Eur. J.* **2005**, *11*, 5975−5987.
(8) Feyel, S.; Schröder, D.; Schwarz, H. Pronounced Cluster-Size Effects: Gas-Phase Reactivity of Bare Vanadium Cluster Cations V_n^+ (n = 1−7) toward Methanol. *J. Phys. Chem. A* **2009**, *113*, 5625−5632.
(9) Schlangen, M.; Schwarz, H. Metal-Dependent Alternative Activation of O-H and C-H Bonds of Methanol: On the Formation and Structure of "Bare" $[M,C,H_3,O]^+$ Complexes (M = Fe, Co, Ni) in the Gas Phase. *Chem. Commun.* **2010**, *46*, 1878−1880.
(10) Schlangen, M.; Schwarz, H. Selective C−H Versus O−H Bond Activation of Ch3oh Upon Electrospraying Methanolic Solutions of MX_2 (M = Fe, Co, Ni; X = Br, I): A DFT Study. *ChemCatChem.* **2010**, *2*, 799−802.
(11) Pratt, R. C.; Stack, T. D. Intramolecular Charge Transfer and Biomimetic Reaction Kinetics in Galactose Oxidase Model Complexes. *J. Am. Chem. Soc.* **2003**, *125*, 8716−8717.
(12) Oh, N. Y.; Suh, Y.; Park, M. J.; Seo, M. S.; Kim, J.; Nam, W. Mechanistic Insight into Alcohol Oxidation by High-Valent Iron-Oxo Complexes of Heme and Nonheme Ligands. *Angew. Chem., Int. Ed.* **2005**, *44*, 4235−4239.
(13) Deng, L.; Ziegler, T. Density Functional Study of C−H and O−H Bond Activation by Transition Metal d^0−Oxo Complexes: 1. Thermodynamic Considerations. *Organometallics* **1996**, *15*, 3011−3021.
(14) Schröder, D.; Shaik, S. S.; Schwarz, H. Two-State Reactivity as a New Concept in Organometallic Chemistrys. *Acc. Chem. Res.* **2000**, *33*, 139−145.

(15) Schlangen, M.; Schwarz, H. Metal-Dependent Alternative Activation of O−H and C−H Bonds of Methanol: On the Formation and Structure of Bare $[M,C,H_3,O]+$ Complexes (M = Fe, Co, Ni) in the Gas Phase. *J. Chem. Soc., Chem. Commun.* **2010**, *46*, 1878−1880.
(16) Kwapien, K.; Sierka, M.; Döbler, J.; Sauer, J. Reactions of H_2, CH_4, C_2H_6, and C_3H_8 with $[(MgO)_n]^+$ Clusters Studied by Density Functional Theory. *ChemCatChem.* **2010**, *2*, 819−826.
(17) Dietl, N. P. R.; Schlangen, M.; Schwarz, H. Thermal Hydrogen-Atom Transfer from Methane: The Role of Radicals and Spin States in Oxo-Cluster Chemistry. *Angew. Chem., Int. Ed.* **2012**, *51*, 5544−5555.
(18) Petrovic, E. D. B. a. M. *Emerging Contaminants from Industrial and Municipal Waste: Removal Technologies* **2008**, 155.
(19) Louwerse, M. J.; Jan Baerends, E. Oxidative Properties of FeO^{2+}: Electronic Structure and Solvation Effects. *Phys. Chem. Chem. Phys.* **2007**, *9*, 156−166.
(20) Michel, C.; Baerends, E. J. What Singles out the FeO^{2+} Moiety? A Density-Functional Theory Study of the Methane-to-Methanol Reaction Catalyzed by the First Row Transition-Metal Oxide Dications $Mo(H_2O)p^{2+}$, M = V−Cu. *Inorg. Chem.* **2009**, *48*, 3628−3638.
(21) Li, J. L.; Zhang, X.; Huang, X. R. Mechanism of Benzene Hydroxylation by High-Valent Bare $Fe^{IV}{=}O^{2+}$: Explicit Electronic Structure Analysis. *Phys. Chem. Chem. Phys.* **2012**, *14*, 246−256.
(22) Yoshizawa, K.; Shiota, Y.; Yamabe, T. Abstraction of the Hydrogen Atom of Methane by Iron−Oxo Species: The Concerted Reaction Path Is Energetically More Favorable. *Organometallics* **1998**, *17*, 2825−2831.
(23) Yoshizawa, K. Two-Step Concerted Mechanism for Alkane Hydroxylation on the Ferryl Active Site of Methane Monooxygenase. *J. Biol. Inorg. Chem.* **1998**, *3*, 318−324.
(24) Yoshizawa, K.; Kamachi, T.; Shiota, Y. A Theoretical Study of the Dynamic Behavior of Alkane Hydroxylation by a Compound I Model of Cytochrome P450. *J. Am. Chem. Soc.* **2001**, *123*, 9806−9816.
(25) Yumura, T.; Yoshizawa, K. Regioselectivity in 2-Methylbutane Hydroxylation Mediated by FeO^+ and FeO^{2+}. *Organometallics* **2001**, *20*, 1397−1407.
(26) Yoshizawa, K. Theoretical Study on Kinetic Isotope Effects in the C-H Bond Activation of Alkanes by Iron-Oxo Complexes. *Coord. Chem. Rev.* **2002**, *226*, 251−259.
(27) Yumura, T.; Amenomori, T.; Kagawa, Y.; Yoshizawa, K. Mechanism for the Formaldehyde to Formic Acid and the Formic Acid to Carbon Dioxide Conversions Mediated by an Iron-Oxo Species. *J. Phys. Chem. A* **2002**, *106*, 621−630.
(28) Kamachi, T.; Yoshizawa, K. A Theoretical Study on the Mechanism of Camphor Hydroxylation by Compound I of Cytochrome P450. *J. Am. Chem. Soc.* **2003**, *125*, 4652−4661.
(29) Yoshizawa, K.; Shiota, Y.; Kihara, N.; Kamachi, T. A Theoretical Study of Reactivity and Regioselectivity in the Hydroxylation of Adamantane by Ferrate(VI). *J. Org. Chem.* **2003**, *68*, 3958−3965.
(30) Yoshizawa, K. Nonradical Mechanism for Methane Hydroxylation by Iron-Oxo Complexes. *Acc. Chem. Res.* **2006**, *39*, 375−382.
(31) Yoshizawa, K.; Shiota, Y.; Yamabe, T. Reaction Pathway for the Direct Benzene Hydroxylation by Iron−Oxo Species. *J. Am. Chem. Soc.* **1998**, *121*, 147−153.
(32) de Visser, S. P.; Oh, K.; Han, A.-R.; Nam, W. Combined Experimental and Theoretical Study on Aromatic Hydroxylation by Mononuclear Nonheme Iron(IV)−Oxo Complexes. *Inorg. Chem.* **2007**, *46*, 4632−4641.
(33) de Visser, S. P.; Ogliaro, F.; Harris, N.; Shaik, S. Multi-State Epoxidation of Ethene by Cytochrome P450: A Quantum Chemical Study. *J. Am. Chem. Soc.* **2001**, *123*, 3037−3047.
(34) de Visser, S. P. Propene Activation by the Oxo-Iron Active Species of Taurine/Alpha-Ketoglutarate Dioxygenase (TauD) Enzyme. How Does the Catalysis Compare to Heme-Enzymes? *J. Am. Chem. Soc.* **2006**, *128*, 9813−9824.
(35) Kumar, D.; Sastry, G. N.; de Visser, S. P. Effect of the Axial Ligand on Substrate Sulfoxidation Mediated by Iron(IV)-Oxo Porphyrin Cation Radical Oxidants. *Chem.—Eur. J.* **2011**, *17*, 6196−6205.
(36) Kumar, D.; Karamzadeh, B.; Sastry, G. N.; de Visser, S. P. What Factors Influence the Rate Constant of Substrate Epoxidation by Compound I of Cytochrome P450 and Analogous Iron(IV)-Oxo Oxidants? *J. Am. Chem. Soc.* **2010**, *132*, 7656−7667.
(37) Porro, C. S.; Sutcliffe, M. J.; de Visser, S. P. Quantum Mechanics/Molecular Mechanics Studies on the Sulfoxidation of Dimethyl Sulfide by Compound I and Compound 0 of Cytochrome P450: Which Is the Better Oxidant? *J. Phys. Chem. A* **2009**, *113*, 11635−11642.
(38) Geng, C. Y.; Ye, S.; Neese, F. Analysis of Reaction Channels for Alkane Hydroxylation by Nonheme Iron(IV)-Oxo Complexes. *Angew. Chem., Int. Ed.* **2010**, *49*, 5717−5720.
(39) Geng, C.; Ye, S.; Neese, F. Does a Higher Metal Oxidation State Necessarily Imply Higher Reactivity toward H-Atom Transfer? A Computational Study of C-H Bond Oxidation by High-Valent Iron-Oxo and -Nitrido Complexes. *Dalton. Trans.* **2014**, *43*, 6079−6086.
(40) Solomon, E. I.; Light, K. M.; Liu, L. V.; Srnec, M.; Wong, S. D. Geometric and Electronic Structure Contributions to Function in Non-Heme Iron Enzymes. *Acc. Chem. Res.* **2013**, *46*, 2725−2739.
(41) Wilson, S. A.; Chen, J.; Hong, S.; Lee, Y.-M.; Clémancey, M.; Garcia-Serres, R.; Nomura, T.; Ogura, T.; Latour, J.-M.; Hedman, B.; et al. $[Fe^{IV}{=}O(TBC)(CH_3CN)]^{2+}$: Comparative Reactivity of Iron(IV)-Oxo Species with Constrained Equatorial Cyclam Ligation. *J. Am. Chem. Soc.* **2012**, *134*, 11791−11806.
(42) Cho, J.; Jeon, S.; Wilson, S. A.; Liu, L. V.; Kang, E. A.; Braymer, J. J.; Lim, M. H.; Hedman, B.; Hodgson, K. O.; Valentine, J. S.; et al. Structure and Reactivity of a Mononuclear Non-Haem Iron(III)-Peroxo Complex. *Nature* **2011**, *478*, 502−505.
(43) Neidig, M. L.; Decker, A.; Choroba, O. W.; Huang, F.; Kavana, M.; Moran, G. R.; Spencer, J. B.; Solomon, E. I. Spectroscopic and Electronic Structure Studies of Aromatic Electrophilic Attack and Hydrogen-Atom Abstraction by Non-Heme Iron Enzymes. *Proc. Natl. Acad. Sci. U. S. A.* **2006**, *103*, 12966−12973.
(44) Decker, A.; Solomon, E. I. Comparison of $Fe^{IV}{=}O$ Heme and Non-Heme Species: Electronic Structures, Bonding, and Reactivities. *Angew. Chem., Int. Ed.* **2005**, *44*, 2252−2255.
(45) Solomon, E. I.; Brunold, T. C.; Davis, M. I.; Kemsley, J. N.; Lee, S. K.; Lehnert, N.; Neese, F.; Skulan, A. J.; Yang, Y. S.; Zhou, J. Geometric and Electronic Structure/Function Correlations in Non-Heme Iron Enzymes. *Chem. Rev.* **2000**, *100*, 235−349.
(46) Shaik, S.; de Visser, S. P.; Kumar, D. External Electric Field Will Control the Selectivity of Enzymatic-Like Bond Activations. *J. Am. Chem. Soc.* **2004**, *126*, 11746−11749.
(47) Ogliaro, F.; Cohen, S.; de Visser, S. P.; Shaik, S. Medium Polarization and Hydrogen Bonding Effects on Compound I of Cytochrome P450: What Kind of a Radical Is It Really? *J. Am. Chem. Soc.* **2000**, *122*, 12892−12893.
(48) Ogliaro, F.; Harris, N.; Cohen, S.; Filatov, M.; Visser, S. P.; Shaik, S. S. A Model "Rebound" Mechanism of Hydroxylation by Cytochrome P450: Stepwise and Effectively Concerted Pathways, and Their Reactivity Patterns. *J. Am. Chem. Soc.* **2000**, *122*, 8977−8989.
(49) Shaik, S.; Kumar, D.; de Visser, S. P. A Valence Bond Modeling of Trends in Hydrogen Abstraction Barriers and Transition States of Hydroxylation Reactions Catalyzed by Cytochrome P450 Enzymes. *J. Am. Chem. Soc.* **2008**, *130*, 10128−10140.
(50) Shaik, S.; Cohen, S.; Wang, Y.; Chen, H.; Kumar, D.; Thiel, W. P450 Enzymes: Their Structure, Reactivity, and Selectivity-Modeled by QM/MM Calculations. *Chem. Rev.* **2010**, *110*, 949−1017.
(51) Meunier, B.; Visser, S. P.; Shaik, S. S. Mechanism of Oxidation Reactions Catalyzed by Cytochrome P450 Enzymes. *Chem. Rev.* **2004**, *104*, 3947−3980.
(52) Shaik, S.; Chen, H.; Janardanan, D. Exchange-Enhanced Reactivity in Bond Activation by Metal-Oxo Enzymes and Synthetic Reagents. *Nat. Chem.* **2011**, *3*, 19−27.
(53) Shaik, S.; Kumar, D.; de Visser, S. P.; Altun, A.; Thiel, W. Theoretical Perspective on the Structure and Mechanism of Cytochrome P450 Enzymes. *Chem. Rev.* **2005**, *105*, 2279−2328.
(54) Sastri, C. V.; Lee, J.; Oh, K.; Lee, Y. J.; Lee, J.; Jackson, T. A.; Ray, K.; Hirao, H.; Shin, W.; Halfen, J. A.; et al. Axial Ligand Tuning of

a Nonheme Iron(IV)-Oxo Unit for Hydrogen Atom Abstraction. *Proc. Natl. Acad. Sci. U. S. A.* **2007**, *104*, 19181−19186.
(55) Klamt, A.; Schüürmann, G. Cosmo: A New Approach to Dielectric Screening in Solvents with Explicit Expressions for the Screening Energy and Its Gradient. *J. Chem. Soc., Perkin Trans.* **1993**, *2*, 799−805.
(56) Grimme, S.; Antony, J.; Ehrlich, S.; Krieg, H. A Consistent and Accurate Ab Initio Parametrization of Density Functional Dispersion Correction (DFT-D) for the 94 Elements H-Pu. *J. Chem. Phys.* **2010**, *132*, 154104.
(57) Li, J. L.; Mata, R. A.; Ryde, U. Large Density-Functional and Basis-Set Effects for the DMSO Reductase Catalyzed Oxo-Transfer Reaction. *J. Chem. Theory Comput.* **2013**, *9*, 1799−1807.
(58) Brittain, D. R. B.; Lin, C. Y.; Gilbert, A. T. B.; Izgorodina, E. I.; Gill, P. M. W.; Coote, M. L. The Role of Exchange in Systematic DFT Errors for Some Organic Reactions. *Phys. Chem. Chem. Phys.* **2009**, *11*, 1138−1142.
(59) Becke, A. D. Density-Functional Thermochemistry. 3. The Role of Exact Exchange. *J. Chem. Phys.* **1993**, *98*, 5648−5652.
(60) Lee, C. T.; Yang, W. T.; Parr, R. G. Development of the Colle-Salvetti Correlation-Energy Formula into a Functional of the Electron-Density. *Phys. Rev. B* **1988**, *37*, 785−789.
(61) Bassan, A.; Blomberg, M. R.; Borowski, T.; Siegbahn, P. E. Theoretical Studies of Enzyme Mechanisms Involving High-Valent Iron Intermediates. *J. Inorg. Biochem.* **2006**, *100*, 727−743.
(62) Weigend, F.; Ahlrichs, R. Balanced Basis Sets of Split Valence, Triple Zeta Valence and Quadruple Zeta Valence Quality for H to Rn: Design and Assessment of Accuracy. *Phys. Chem. Chem. Phys.* **2005**, *7*, 3297−3305.
(63) Furche, F.; Ahlrichs, R.; Hättig, C.; Klopper, W.; Sierka, M.; Weigend, F. Turbomole. *Wiley Interdiscip. Rev.: Comput. Mol. Sci.* **2014**, *4*, 91−100.
(64) Becke, A. D. Density-Functional Exchange-Energy Approximation with Correct Asymptotic Behavior. *Phys. Rev. A* **1988**, *38*, 3098−3100.
(65) Perdew, J. P. Density-Functional Approximation for the Correlation Energy of the Inhomogeneous Electron Gas. *Phys. Rev. B* **1986**, *33*, 8822−8824.
(66) Becke, A. D. A New Mixing of Hartree-Fock and Local Density-Functional Theories. *J. Chem. Phys.* **1993**, *98*, 1372−1377.
(67) Tarnopolsky, A.; Karton, A.; Sertchook, R.; Vuzman, D.; Martin, J. M. L. Double-Hybrid Functionals for Thermochemical Kinetics. *J. Phys. Chem. A* **2008**, *112*, 3−8.
(68) Neese, F. The Orca Program System. *Wiley Interdiscip. Rev.: Comput. Mol. Sci.* **2012**, *2*, 73−78.
(69) Kohn, W.; Sham, L. J. Self-Consistent Equations Including Exchange and Correlation Effects. *Phys. Rev.* **1965**, *140*, 1133−&.
(70) Perdew, J. P.; Burke, K.; Ernzerhof, M. Generalized Gradient Approximation Made Simple. *Phys. Rev. Lett.* **1996**, *77*, 3865−3868.
(71) Tao, J.; Perdew, J. P.; Staroverov, V. N.; Scuseria, G. E. Climbing the Density Functional Ladder: Nonempirical Meta-Generalized Gradient Approximation Designed for Molecules and Solids. *Phys. Rev. Lett.* **2003**, *91*, 146401.
(72) Cohen, A. J.; Handy, N. C. Dynamic Correlation. *Mol. Phys.* **2001**, *99*, 607−615.
(73) Chai, J. D.; Head-Gordon, M. Long-Range Corrected Hybrid Density Functionals with Damped Atom-Atom Dispersion Corrections. *Phys. Chem. Chem. Phys.* **2008**, *10*, 6615−6620.
(74) Xu, X.; Goddard, W. A., 3rd From the Cover: The X3LYP Extended Density Functional for Accurate Descriptions of Nonbond Interactions, Spin States, and Thermochemical Properties. *Proc. Natl. Acad. Sci. U. S. A.* **2004**, *101*, 2673−2677.
(75) Adamo, C.; Barone, V. Toward Reliable Density Functional Methods without Adjustable Parameters: The PBE0Model. *J. Chem. Phys.* **1999**, *110*, 6158−6170.
(76) Adamo, C.; Barone, V. Exchange Functionals with Improved Long-Range Behavior and Adiabatic Connection Methods without Adjustable Parameters: The MPW and MPW1PW Models. *J. Chem. Phys.* **1998**, *108*, 664−675.
(77) Quintal, M. M.; Karton, A.; Iron, M. A.; Boese, A. D.; Martin, J. M. L. Benchmark Study of DFT Functionals for Late-Transition-Metal Reactions. *J. Phys. Chem. A* **2006**, *110*, 709−716.
(78) Zhao, Y.; Truhlar, D. G. The M06 Suite of Density Functionals for Main Group Thermochemistry, Thermochemical Kinetics, Noncovalent Interactions, Excited States, and Transition Elements: Two New Functionals and Systematic Testing of Four M06-Class Functionals and 12 Other Functionals. *Theor. Chem. Acc.* **2007**, *120*, 215−241.
(79) Zhao, Y.; Truhlar, D. G. Design of Density Functionals That Are Broadly Accurate for Thermochemistry, Thermochemical Kinetics, and Nonbonded Interactions. *J. Phys. Chem. A* **2005**, *109*, 5656−5667.
(80) Goerigk, L.; Grimme, S. Efficient and Accurate Double-Hybrid-Meta-GGA Density Functionals-Evaluation with the Extended GMTKN30 Database for General Main Group Thermochemistry, Kinetics, and Noncovalent Interactions. *J. Chem. Theory Comput.* **2011**, *7*, 291−309.
(81) Grimme, S. Semiempirical Hybrid Density Functional with Perturbative Second-Order Correlation. *J. Chem. Phys.* **2006**, *124*, 034108.
(82) Karton, A.; Tarnopolsky, A.; Lamère, J.-F. o.; Schatz, G. C.; Martin, J. M. L. Highly Accurate First-Principles Benchmark Data Sets for the Parametrization and Validation of Density Functional and Other Approximate Methods. Derivation of a Robust, Generally Applicable, Double-Hybrid Functional for Thermochemistry and Thermochemical Kinetics. *J. Phys. Chem. A* **2008**, *112*, 12868−12886.
(83) Watts, J. D.; Gauss, J.; Bartlett, R. J. Coupled-Cluster Methods with Noniterative Triple Excitations for Restricted Open-Shell Hartree-Fock and Other General Single Determinant Reference Functions. Energies and Analytical Gradients. *J. Chem. Phys.* **1993**, *98*, 8718−8733.
(84) Frisch, M. J.; Trucks, G. W.; Schlegel, H. B.; Scuseria, G. E.; Robb, M. A.; Cheeseman, J. R.; Montgomery, J. A., Jr.; Vreven, T.; Kudin, K. N.; Burant, J. C.; Millam, J. M.; Iyengar, S. S.; Tomasi, J.; Barone, V.; Mennucci, B.; Cossi, M.; Scalmani, G.; Rega, N.; Petersson, G. A.; Nakatsuji, H.; Hada, M.; Ehara, M.; Toyota, K.; Fukuda, R.; Hasegawa, J.; Ishida, M.; Nakajima, T.; Honda, Y.; Kitao, O.; Nakai, H.; Klene, M.; Li, X.; Knox, J. E.; Hratchian, H. P.; Cross, J. B.; Adamo, C.; Jaramillo, J.; Gomperts, R.; Stratmann, R. E.; Yazyev, O.; Austin, A. J.; Cammi, R.; Pomelli, C.; Ochterski, J. W.; Ayala, P. Y.; Morokuma, K.; Voth, G. A.; Salvador, P.; Dannenberg, J. J.; Zakrzewski, V. G.; Dapprich, S.; Daniels, A. D.; Strain, M. C.; Farkas, O.; Malick, D. K.; Rabuck, A. D.; Raghavachari, K.; Foresman, J. B.; Ortiz, J. V.; Cui, Q.; Baboul, A. G.; Clifford, S.; Cioslowski, J.; Stefanov, B. B.; Liu, G.; Liashenko, A.; Piskorz, P.; Komaromi, I.; Martin, R. L.; Fox, D. J.; Keith, T.; Al-Laham, M. A.; Peng, C. Y.; Nanayakkara, A.; Challacombe, M.; Gill, P. M. W.; Johnson, B.; Chen, W.; Wong, M. W.; Gonzalez, C.; Pople, J. A. *Gaussian 03*, revision E.01; Gaussian Inc.: Wallingford, CT, 2004.
(85) Sun, X.; Geng, C.; Huo, R.; Ryde, U.; Bu, Y.; Li, J. Large Equatorial Ligand Effects on C−H Bond Activation by Nonheme Iron(IV)-Oxo Complexes. *J. Phys. Chem. B* **2014**, *118*, 1493−1500.
(86) Janardanan, D.; Usharani, D.; Chen, H.; Shaik, S. Modeling C-H Abstraction Reactivity of Nonheme Fe(IV)O Oxidants with Alkanes: What Role Do Counter Ions Play? *J. Phys. Chem. Lett.* **2011**, *2*, 2610−2617.
(87) Usharani, D.; Lacy, D. C.; Borovik, A. S.; Shaik, S. Dichotomous Hydrogen Atom Transfer vs Proton-Coupled Electron Transfer During Activation of X−H Bonds (X = C, N, O) by Nonheme Iron−Oxo Complexes of Variable Basicity. *J. Am. Chem. Soc.* **2013**, *135*, 17090−17104.
(88) de Visser, S. P. What Factors Influence the Ratio of CH Hydroxylation Versus CC Epoxidation by a Nonheme Cytochrome P450 Biomimetic? *J. Am. Chem. Soc.* **2006**, *128*, 15809−15818.
(89) Pau, M. Y. M.; Davis, M. I.; Orville, A. M.; Lipscomb, J. D.; Solomon, E. I. Spectroscopic and Electronic Structure Study of the Enzyme−Substrate Complex of Intradiol Dioxygenases: Substrate Activation by a High-Spin Ferric Non-Heme Iron Site. *J. Am. Chem. Soc.* **2007**, *129*, 1944−1958.

(90) Decker, A.; Rohde, J.-U.; Klinker, E. J.; Wong, S. D.; Que, L.; Solomon, E. I. Spectroscopic and Quantum Chemical Studies on Low-Spin $Fe^{IV}O$ Complexes: Fe−O Bonding and Its Contributions to Reactivity. *J. Am. Chem. Soc.* **2007**, *129*, 15983−15996.
(91) Leeladee, P.; Jameson, G. N. L.; Siegler, M. A.; Kumar, D.; de Visser, S. P.; Goldberg, D. P. Generation of a High-Valent Iron Imido Corrolazine Complex and NR Group Transfer Reactivity. *Inorg. Chem.* **2013**, *52*, 4668−4682.
(92) Mosley, J. D.; Cheng, T. C.; McCoy, A. B.; Duncan, M. A. Infrared Spectroscopy of the Mass 31 Cation: Protonated Formaldehyde vs Methoxy. *J. Phys. Chem. A* **2012**, *116*, 9287−9294.
(93) Groves, J. T.; Mcclusky, G. A. Aliphatic Hydroxylation via Oxygen Rebound-Oxygen-Transfer Catalyzed by Iron. *J. Am. Chem. Soc.* **1976**, *98*, 859−861.
(94) Cho, K.-B.; Shaik, S.; Nam, W. Theoretical Investigations into C−H Bond Activation Reaction by Nonheme Mnivo Complexes: Multistate Reactivity with No Oxygen Rebound. *J. Phys. Chem. Lett.* **2012**, *3*, 2851−2856.
(95) Li, J.; Geng, C.; Huang, X.; Sun, C.; Barrier-Free, A. Atomic Radical-Molecule Reaction: F + Propene. *J. Chem. Theory Comput.* **2006**, *2*, 1551−1564.
(96) Lundberg, M.; Siegbahn, P. E. Quantifying the Effects of the Self-Interaction Error in DFT: When Do the Delocalized States Appear? *J. Chem. Phys.* **2005**, *122*, 224103.
(97) Schröder, D.; Schwarz, H. C−H and C−C Bond Activation by Bare Transition-Metal Oxide Cations in the Gas Phase. *Angew. Chem., Int. Ed.* **1995**, *34*, 1973−1995.
(98) Yoshizawa, K.; Kagawa, Y. Reaction Pathways for the Oxidation of Methanol to Formaldehyde by an Iron−Oxo Species. *J. Phys. Chem. A* **2000**, *104*, 9347−9355.
(99) Ess, D. H.; Houk, K. N. Activation Energies of Pericyclic Reactions: Performance of DFT, MP2, and CBS-QB3Methods for the Prediction of Activation Barriers and Reaction Energetics of 1,3-Dipolar Cycloadditions, and Revised Activation Enthalpies for a Standard Set of Hydrocarbon Pericyclic Reactions. *J. Phys. Chem. A* **2005**, *109*, 9542−9553.
(100) Bernardo, C. P.; Bauman, N.; Piecuch, P.; Silva, P. Evaluation of Density Functional Methods on the Geometric and Energetic Descriptions of Species Involved in Cu^{+}-Promoted Catalysis. *J. Mol. Model.* **2013**, *19*, 5457−5467.
(101) Thomson, L. M.; Hall, M. B. Theoretical Study of the Thermal Decomposition of N,N′-Diacyl-N,N′-Dialkoxyhydrazines: A Comparison of HF, MP2, and DFT. *J. Phys. Chem. A* **2000**, *104*, 6247−6252.
(102) Izgorodina, E. I.; Coote, M. L.; Radom, L. Trends in R−X Bond Dissociation Energies (R = Me, Et, *i*-Pr, *t*-Bu; X = H, CH_3, OCH_3, OH, F): A Surprising Shortcoming of Density Functional Theory. *J. Phys. Chem. A* **2005**, *109*, 7558−7566.
(103) Kang, R. H.; Chen, H.; Shaik, S.; Yao, J. N. Assessment of Theoretical Methods for Complexes of Gold(I) and Gold(III) with Unsaturated Aliphatic Hydrocarbon: Which Density Functional Should We Choose? *J. Chem. Theory Comput.* **2011**, *7*, 4002−4011.
(104) Reiher, M.; Salomon, O.; Hess, B. A. Reparameterization of Hybrid Functionals Based on Energy Differences of States of Different Multiplicity. *Theor. Chem. Acc.* **2001**, *107*, 48−55.
(105) Jensen, K. P.; Ryde, U. Theoretical Prediction of the Co−C Bond Strength in Cobalamins. *J. Phys. Chem. A* **2003**, *107*, 7539−7545.
(106) Heimdal, J.; Kaukonen, M.; Srnec, M.; Rulisek, L.; Ryde, U. Reduction Potentials and Acidity Constants of Mn Superoxide Dismutase Calculated by QM/MM Free-Energy Methods. *ChemPhysChem* **2011**, *12*, 3337−3347.
(107) Siegbahn, P. E. M.; Blomberg, M. R. A. Energy Diagrams for Water Oxidation in Photosystem II Using Different Density Functionals. *J. Chem. Theory Comput.* **2013**, *10*, 268−272.
(108) Sun, X. L.; Huang, X. R.; Li, J. L.; Huo, R. P.; Sun, C. C. Mechanism Insights of Ethane C-H Bond Activations by Bare $[Fe^{III}{=}O]^{+}$: Explicit Electronic Structure Analysis. *J. Phys. Chem. A* **2012**, *116*, 1475−1485.
(109) Lai, W.; Li, C.; Chen, H.; Shaik, S. Hydrogen-Abstraction Reactivity Patterns from A to Y: The Valence Bond Way. *Angew. Chem., Int. Ed.* **2012**, *51*, 5556−5578.